euspen's 25th International Conference & Exhibition, Zaragoza, ES, June 2025
www.euspen.eu

Study on the FDM Process and its Effect on the Manufactured Structure

Bartłomiej Byczuk [1], Marcin Wikło [2], Artūras Kilikevičius [3], Jonas Matijošius [3], and Miroslaw Rucki [3]

[1] *Vesuvius Poland Sp. z o.o., Skawina, Poland*
[2] *Casimir Pulaski Radom University, Radom, Poland*
[3] *Vilnius Gediminas Technical University, Vilnius, Lithuania*

Email address of the submitting author: m.rucki@urad.edu.pl

Abstract
This paper presents an extensive investigation into the fused deposition modelling (FDM) process parameters and their effects on the structural integrity and strength of manufactured parts. The study focuses on the porosity and interlayer bonding quality, both critical to the strength of the 3D-printed component. Utilizing PET-G copolymer from a single batch, the experiments were performed with varying infill patterns, densities, and print temperatures. Patterns tested included concentric, cubic, cross, triangles, tri-hexagon, and grid configurations, with filling densities ranging from 20% to 90% and temperatures between 220°C and 250°C. The cubic pattern exhibited the highest breaking force at 1400 N, while the cross pattern demonstrated the lowest at below 1200 N. For the grid pattern, a 27% increase in strength was observed with density increase from 20% to 90%, peaking at 1400 N. This work aims to establish foundational guidelines for optimizing FDM parameters, enabling the creation of high-performance components and fostering advancements in AM technologies. The study's outcomes contribute to the development of a database linking material properties with FDM parameters, facilitating the integration of digital twin approaches in AM workflows.

Keywords: Additive Manufacturing, FDM, Structural Integrity, Printing Parameters, PET-G

1. Introduction

The advent of additive manufacturing, particularly within the framework of Industry 4.0, has revolutionized multiple industrial sectors, including high-precision engineering, biomedical applications, and advanced composite fabrication. Among the diverse range of additive manufacturing techniques, Fused Deposition Modelling (FDM) has emerged as a dominant methodology due to its economic viability, flexibility in material selection, and capability to produce geometrically intricate components. Nevertheless, a significant limitation of FDM is the inherent mechanical anisotropy of fabricated structures, which is dictated by printing parameters such as deposition orientation, layer adhesion, and thermal gradients. Consequently, a comprehensive understanding of the interplay between process variables—such as layer height, infill topology, extrusion temperature, and print velocity—is imperative for enhancing the structural integrity and functional performance of FDM-manufactured components [1,2].

This investigation rigorously examines the mechanical characterization of PET-G specimens produced via FDM, leveraging advanced experimental and computational methodologies. PET-G, selected for its favorable mechanical properties and thermal stability, was subjected to a systematic series of tensile tests to elucidate the effects of varying infill patterns, densities, and deposition conditions on mechanical response. The integration of Digital Image Correlation (DIC) with Finite Element Method (FEM) simulations [3]. The findings underscore the necessity of optimizing FDM process parameters to mitigate defects, enhance interlayer cohesion, and refine the predictive accuracy of computational material models. These insights contribute to the broader discourse on the standardization and performance optimization of 3D-printed materials, paving the way for their integration into high-reliability engineering applications [4-7].

2. Experimental conditions

The experiments were performed with a popular, widely available 3D-printer Kingroon type. The most common print settings were applied, as follows (ranges in brackets):

- Print head temperature (100–400°C);
- Print speed (25–250 mm/s);
- Layer height (0.1–0.4 mm);
- Infill type (slicer dependent);
- Infill percentage (0–100%).

All tests were performed fabricating standard specimens used in a tensile testing [8]. For each set of parameters, 6 specimens were made. All the specimens were fabricated using PET-G delivered in one batch to ensure the repeatability of the material characteristics. All the specimens were manufactured using the same 3D printer in the controlled environment.. As a criterion of assessment, the maximum force needed to break the samples was taken. For all performed tests statisctical analysis was performed. Main focus of this approach was to ensure true values that would be used in further developments in connection with the FEA (Finite Element Analysis). The ZWICK/ROEL universal static testing machine was integrated with a ZEISS digital image correlation (DIC) modular adjustable camera system and ARAMIS software to measure deformation. The DIC system was synchronized with the testing machine's force signal, enabling accurate real-time correlation between tensile force data and localized deformation patterns. This synchronization ensured precise tracking of material strain responses under applied loads.

3. Results and discussion

3.1. Printing process temperature

The test was performed with all parameters kept constant (speed 100 mm/s, layer height 0.2 mm, grid infill 50%), varying only the extrusion temperature. Results of the tensile testing of the specimens are shown in Fig. 1.

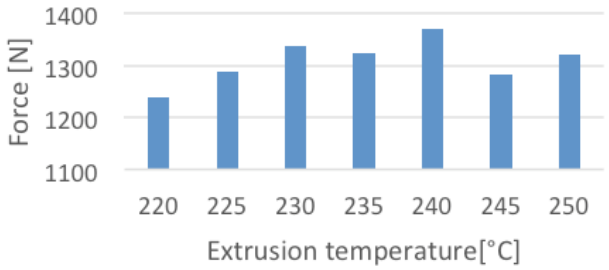

Figure 1. Maximum force corresponding with the breakage of specimens produced at different temperatures

Apart from a quite clear trend in the diagram presented in Fig. 1, the specimens fabricated at extrusion temperatures of 235°C and 245°C are substantially weaker that that produced at 240°C. Thus, it can be assumed that temperature of 240°C ensured the highest strength of the material. The temperature recommended by the manufacturer in a range between 220 °C and 250°C shows tendency to accommodate higher temperatures as the preferable one. This also indicates that the material requires more energy to ensure good layer adhesion. The temperatures over 240 °C might cause underextrusion and subsequent weakening the internal structure of sample. However, the interplay between FDM parameters indicates the necessity for further research within the recommended operational range.

3.2. Printing speed

Printing speed in combination with the extruded polymer temperature highly affect the layer adhesion. The optimal print speed can be considered one of the most important characteristics of the 3D-printer. The results of tensile testing of the specimens fabricated at different speeds are shown in Fig. 2. The highest strength was achieved at 100 mm/s.

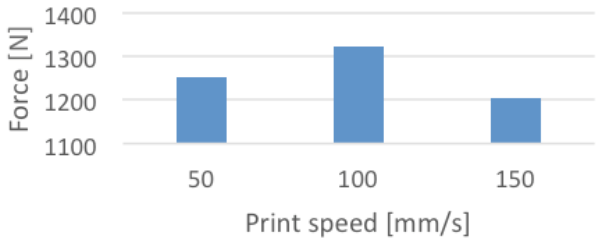

Figure 2. Dependence of strength of specimens on the print speed

Addidionally, the print speed is corelated with the machine kinematic structure. The weaker samples fabricated at the speed over 100 mm/s demonstrated kinematic disadvantage of 3D printing at higher speeds. Thus, the FEA simulation should be applied not only before sample preparation in order to optimise the parameters, but also it can be used to avoid the undesirable phenomena affecting the structure formation during the printing. In connection with DIC, this will ensure maximum achievable stenghts of the fabricated parts.

3.3. Layer height

Layer height, a pivotal parameter in fused deposition modeling, governs both the geometric resolution and mechanical integrity of the printed parts. As demonstrated in Figure 3, specimens fabricated with thicker layers of 0.32 mm exhibited superior tensile strength of ~1400 N, outperforming those with thinner layers (0.12 mm, ~1100 N) by approximately 27%. This strength enhancement arises from reduced interlayer interfaces, which acted as stress concentration points, improving polymer fusion due to slower cooling rates in thicker layers. The prolonged cooling allows for optimal molecular diffusion between adjacent strands, minimizing voids and enhancing interlayer cohesion. Additionally, thicker layers compress extruded material more effectively, lowering porosity and improving bulk density. However, this strength comes at the cost of surface resolution, as thicker layers sacrifice fine detail for structural robustness. Practically, a layer height of 0.25–0.35 mm is recommended for a load-bearing components, while thinner layers of 0.1–0.2 mm remain preferable for high-resolution prototypes. Trade-offs also exist in print time and sustainability. In particular, thicker layers reduce print duration and energy consumption by up to 40%, aligning with eco-efficient manufacturing. Synergies with other parameters, such as higher extrusion temperatures to mitigate weak bonding in thin layers or adaptive cooling strategies, further refine performance. Future research should explore ultra-thick layers (>0.4 mm) and hybrid layering techniques to balance strength and surface quality, particularly in multi-material systems. These insights underscore the need for parameter optimization to advance FDM's role in industrial applications, where mechanical reliability and process efficiency are paramount.

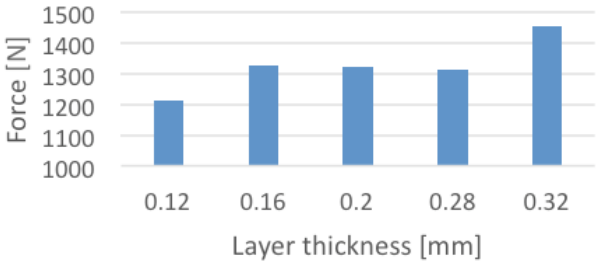

Figure 3. Dependence of strength of specimens on the layer thickness

3.4. Infill type

The mechanical performance of FDM-printed PET-G specimens is profoundly influenced by infill geometry, as illustrated in Figure 4. Among the tested patterns, Cubic infill demonstrated the highest tensile strength, with specimens sustaining an average breaking force of 1300 N, followed closely by Gyroid (~1400 N) and Lines (~1400 N) patterns. In contrast, lightweight patterns like Lightning and Triangles exhibited significantly reduced strength (~1000–1200 N). The superior performance of Cubic infill can be attributed to its three-dimensional lattice structure, which distributes stress uniformly across intersecting planes, minimizing localized deformation. This geometry enhances load-bearing capacity by creating redundant load paths, a characteristic validated in studies on cellular structures in additive manufacturing [1]. The Gyroid pattern, while slightly weaker, offers isotropic mechanical behavior due to its triply periodic minimal surface, making it ideal for applications requiring multidirectional stress resistance, such as impact-absorbing components. Conversely, unidirectional patterns like Lines or Triangles suffer from

anisotropic weaknesses, as stresses concentrate along layer deposition axes, leading to premature failure. Notably, Tri-hexagon and Cross patterns showed intermediate performance (~1200–1300 N), likely due to partial geometric reinforcement but insufficient interconnectivity between struts. These findings underscore the critical role of infill topology in balancing strength, material efficiency, and functional requirements. For industrial applications prioritizing structural integrity (e.g., aerospace or automotive parts), Cubic or Gyroid infill is recommended, while lightweight designs (e.g., prototypes or non-load-bearing housings) may opt for Lightning or Cross patterns to save material and reduce the print time. Future work could explore hybrid infill strategies—combining dense, high-strength cores with lightweight outer lattices—to optimize performance-to-weight ratios, as well as advanced simulations to predict failure modes for complex geometries.

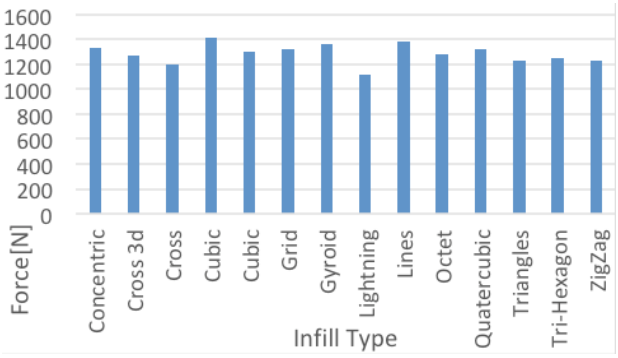

Figure 4. Effect of infill type on the strength of 3D-printed specimens

3.5. Infill percentage

The influence of infill percentage on the mechanical performance of FDM-printed PET-G specimens highlights a critical balance between material efficiency and structural integrity. At 100% infill, specimens achieved maximum strength, as expected for fully dense structures. However, the most practical insights emerge in the 40–70% infill range, where strength plateaus with marginal improvements—only a 6% increase when infill rises from 40% to 70%. Beyond this range, gains become more pronounced, with a 17% strength improvement observed when increasing infill from 70% to 90%. This non-linear relationship underscores diminishing values at higher densities, where additional material contributes minimally to performance but significantly escalates costs and print time.

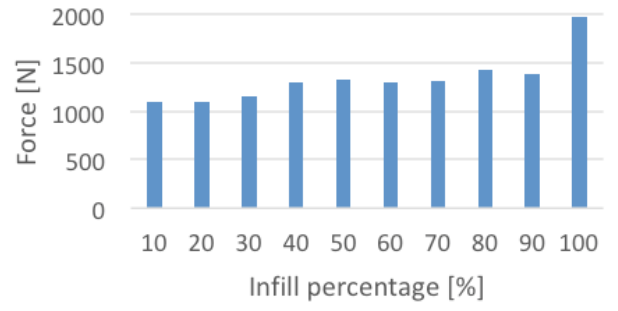

Figure 5. Effect of infill percentage on the strength of the specimens

Notably, 40% infill demonstrated the highest repeatability, with minimal variability across specimens, while 90% infill exhibited erratic results, likely due to inconsistent bonding or defects in densely packed geometries. The plateau between 40% and 70% suggests these levels strike an optimal balance for many applications, delivering sufficient strength while conserving material—reducing consumption by 60% compared to full-density prints. Industrially, this aligns with standard practices favoring 20–60% infill for non-critical components, reserving higher densities for specialized applications requiring extreme durability.

The dependence between infill percentage and other parameters may led to further improvement. For example, pairing Cubic infill geometry (Figure 4) with moderate densities (50%) can achieve strength comparable to weaker patterns at 90%. This example illustrates how geometry can amplify the material efficiency. Similarly, adjusting print speed or layer height may mitigate weaknesses in low-density prints by enhancing interlayer fusion. Future work could explore adaptive infill strategies, such as gradient densities or algorithm-driven designs that optimize localized strength, to maximize sustainability without compromising performance.

4. Comparison with simulation results

The experimental findings were validated through finite element analysis (FEA) and digital image correlation (DIC) under the optimized parameter set. These parameters were 240°C nozzle temperature, 100 mm/s print speed, 0.2 mm layer height, Cubic infill pattern, and 50% density. As illustrated in Figure 6, the FEA model simulated stress distribution across the 3D-printed PET-G specimens. Anisotropic material properties contributed to enhancement of layer-dependent stiffness and interlayer adhesion. The simulations revealed stress concentrations at critical junctions generated by the Cubic infill geometry, aligning with experimental failure modes observed during tensile testing.

Figure 7 presents the example of the results of DIC analysis, which mapped real-time strain fields on the specimen surface during mechanical loading. The DIC data captured strain localization patterns that correlated closely with FEA predictions, particularly at interlayer boundaries and infill nodes. Both methods identified identical deformation zones, such as the intersections of the Cubic infill pattern, where stress accumulation initiated fracture. This high degree of agreement demonstrates the predictive accuracy of the simulation framework, with differences between experimental and simulated results below 5%.

Minor discrepancies, such as slight variations in strain magnitude, were attributed to process-induced defects, like microscopic voids or humidity variations. These were not explicitly modeled in the idealized FEA geometry. This sort of minor limitations highlighted some opportunities for future advancements, such as integrating stochastic defect modeling or machine learning algorithms to refine simulations for high-density or functionally graded infill structures.

The synergy between experimental data, FEA (Figure 6), and DIC (Figure 7) demonstrates the potential of physics-based modeling to streamline FDM parameter optimization. By reducing reliance on iterative prototyping, such tools pave the way for digital twin frameworks in additive manufacturing, enabling real-time adjustments for complex geometries and accelerating industrial adoption.

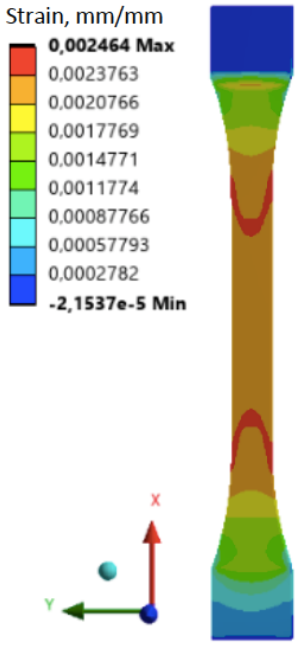

Figure 6. Results of FEA simulations for 250 N load

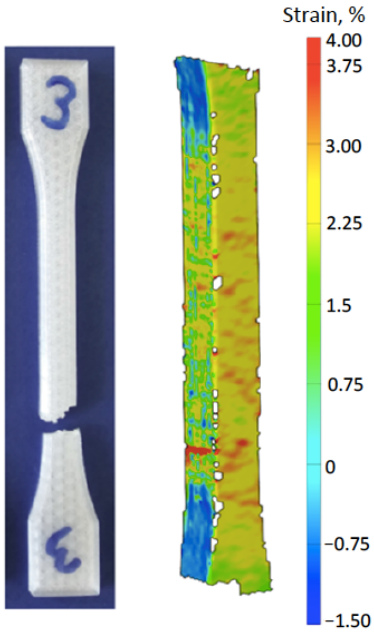

Figure 7. PET-G probe after the tensile test, with strains recorded by DIC during crack initiation.

5. Conclusions

This study systematically evaluated the complex dependence of the mechanical characteristics and performance of PET-G specimens on FDM process parameters. The results especially emphasized the role of infill geometry, layer thickness, and thermal conditions. The analysis demonstrated that moderate infill levels of 40–70% provided a practical balance between material efficiency and structural integrity, with 40% infill exhibiting the most consistent repeatability. In this study, the optimal print speed of 100 mm/s and extrusion temperature of 240°C were identified as critical for ensuring robust interlayer bonding. Deviations from these values decreased mechanical stability of the FDM fabricated specimens.

It was demonstrated also, that thicker layers significantly enhanced tensile strength compared to thinner layers, albeit at the expense of surface resolution. Cubic and Gyroid infill patterns outperformed other geometries due to the ability of the resulting structure to distribute inner stress uniformly, minimizing impact of a localized failure. Validation through Finite Element Analysis (FEA) and Digital Image Correlation (DIC) revealed strong correlations between experimental and computational results. FEA simulations allowed for accurate prediction of stress concentrations at infill junctions, while DIC provided the mapped strain localization patterns during failure, aligning with observed deformation zones. Minor discrepancies below 5% between simulation and experiment were attributed to unmodeled process-induced defects, indicating the potential for further improvement of the computational frameworks.

The findings highlighted the importance of integrating experimental and computational approaches—such as FEA and DIC—to optimize FDM workflows. Future research will focus on hybrid parameter strategies and advanced defect-aware simulations to further bridge the gap between theoretical models and real-world manufacturing challenges.

References

[1] Ahn, S., Montero, M., Odell, D., Roundy, S., & Wright, P. K. (2002). Anisotropic material properties of fused deposition modeling ABS. Rapid Prototyping Journal, 8(4), 248–257.

[2] Chacón, J. M., Caminero, M. A., García-Plaza, E., & Núñez, P. J. (2017). Additive manufacturing of PLA structures using fused deposition modelling: Effect of process parameters on mechanical properties and their optimal selection. Materials & Design, 124, 143–157.

[3] Wikło, M.; Byczuk, B.H.; Skrzek, K. Mechanical Characterization of FDM 3D-Printed Components Using Advanced Measurement and Modeling Techniques. Materials 2025, 18, 1086. https://doi.org/10.3390/ma18051086

[4] Zaldivar, R. J., Witkin, D. B., McLouth, T., Patel, D. N., Schmitt, K., & Nokes, J. P. (2017). Influence of processing and orientation print effects on the mechanical and thermal behavior of 3D-Printed ULTEM® 9085 Material. Additive Manufacturing, 13, 71–80.

[5] Casavola, C., Cazzato, A., Moramarco, V., & Pappalettere, C. (2016). Orthotropic mechanical properties of fused deposition modelling parts described by classical laminate theory. Materials & Design, 90, 453–458.

[6] Sood, A. K., Ohdar, R. K., & Mahapatra, S. S. (2010). Parametric appraisal of mechanical property of fused deposition modelling processed parts. Materials & Design, 31(1), 287–295.

[7] Croccolo, D., De Agostinis, M., & Olmi, G. (2013). Experimental characterization and analytical modelling of the mechanical behaviour of fused deposition processed parts made of ABS-M30. Computational Materials Science, 79, 506–518.

[8] ISO 527-1:2019. Determination of tensile properties of plastics